URSI GASS 2021, Rome, Italy, 28 August - 4 September 2021

3D Printed 18 GHz to 28 GHz Horn Antenna and Gradient Index of Refraction Lens

Ian Goode* and Carlos E. Saavedra
Department of Electrical and Computer Engineering
Queen's University, Kingston, ON, Canada
ian.goode@queensu.ca, saavedra@queensu.ca

Abstract

A 3D printed K-band horn antenna with a planar GRIN (gradient index of refraction) lens is reported. The horn antenna has elliptically flared sidewalls that are 3D printed using polylactic acid (PLA) and covered in copper tape. The planar GRIN lens models the phase delay profile of a spherical Luneburg lens, with a gain increase of 5 dB or better across the 18 GHz to 28 GHz band and is printed using ECO-ABS. By moving a dielectric cylinder with $\varepsilon_r = 2.4$ on the inner surface of the lens, a beam-steering angle of $\pm 5°$ is demonstrated.

1 Introduction

Additive manufacturing has allowed for rapid prototyping of topologies that are difficult or costly to manufacture through conventional methods. This has been demonstrated at microwave and mm-wave frequencies for the fabrication of antennas [1, 2], lenses [3], and other waveguide components [4]. To aid in the design of 3D printed microwave components the electrical properties of commonly used polymers were measured in [5] and the effects of surface roughness of conductive printing materials were shown in [6]. However, printing with non-conductive materials is attractive as it is more readily available, less expensive, and easier to operate than metal 3D printing. To make conductive components while printing in plastic conductive filament can be used [7], conductive ink can be applied while printing [2], parts can be spray coated and electro-plated after printing [1], or printed parts can be covered with metallic tape [8].

Lenses are used to increase the gain of antennas and allow for beam-steering [3, 9]. Typically, spherical Luneburg lenses have been fabricated by nesting shells of materials with different dielectric constants [10] or by milling multiple holes through a uniform material to change permittivity [11]. 3D printing allows for a lens to be printed out of single material by varying the density of the material to achieve the desired permittivity profile [3]. Using this technique complex lens topologies can be printed to create the desired phase-delay for optimal beam-forming, referred to as gradient index of refection (GRIN) lenses. GRIN lenses have been implemented inside the aperture of horn antennas [1] or outside the aperture as planar structures [12]. Lensed antennas can also be used for beam-steering by varying the permittivity profile along the radiation path. This has been seen by mechanically rotating lenses [11] or by adding dielectric fluid to regions of a lens to vary the propagation velocity [9].

This work proposes a 3D printed WR-42 horn antenna that covers 18 GHz to 28 GHz. It is printed from PLA (polylactic acid), is coated on the inside with copper tape and is assembled with joints at the corners of the waveguide. The radiation pattern of this horn is enhanced using a 3D printed GRIN lens based on the permittivity profile of a Luneburg lens, printed with the ECO-ABS filament. Axial beam-stabilization is examined using a PETG (polyethylene terephthalate glycol) 3D printed cylinder to emulate the movement of a mineral oil droplet. It is known that axial vibrations can cause link loss in long-range wireless systems that use high gain antennas, as the transmitted beam points away from the target. A fluid droplet could passively move in the opposite direction of the perturbation relative to the lens to cancel it. Here the PETG cylinder is manually moved to show the beam-steering compensation effect.

2 Horn and Lens Design and Fabrication

The design of this horn was done in three parts: the design of a WR-42 (10.7 mm by 4.3 mm) horn antenna that could be 3D printed and metalized using adhesive backed copper foil, the design of the GRIN lens, and the design of a pocketed GRIN lens with a PETG cylinder for beam-steering. All portions of this design were simulated in ANSYS HFSS and the models for the permittivity of the material used in the lens was measured in [5].

The horn antenna consists of a WR-42 waveguide with flares following an elliptical contour seen in Fig. 1. The contours from the $\vec{E}$ and $\vec{H}$ walls of the waveguide were chosen to give an equal beam-width in both the $\vec{E}$ and $\vec{H}$ radiation cut planes. The horn walls were modeled as smooth copper surfaces.

The GRIN lens was designed to have the same phase delay profile as a Luneburg lens and be radially symmetric.

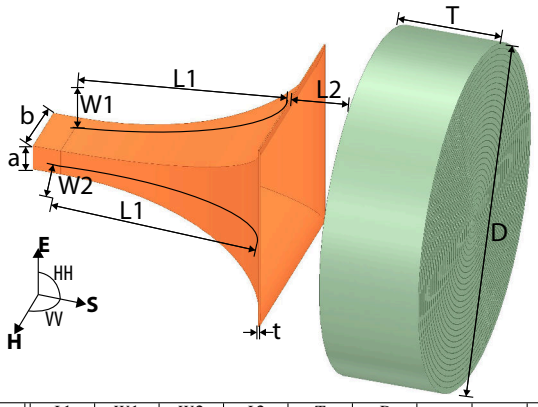

var.	$L1$	$W1$	$W2$	$L2$	T	D	t	a	b
[mm]	40.0	15.7	12.5	15.0	17.9	61.0	1.0	4.3	10.7

Figure 1. Model of the horn antenna and GRIN lens showing the dimensions of each and the radiation pattern cut planes relative to the shape of the horn

The GRIN lens is cylindrical, with a uniform permittivity throughout the height of the lens. This was modeled in HFSS as concentric nested cylinders with varied dielectric constants and a thickness of 2 mm. The dimensions of the GRIN lens are seen in Fig. 1 with the largest dielectric constant being $\varepsilon_r = 2.7$, which is the relative permittivity of Dremel ECO-ABS (a modified PLA).

To see the beam-steering effect that could be observed by moving a homogenous piece of a dielectric material, a PETG ($\varepsilon_r = 2.4$) cylinder was added to the horn side of the lens. The PETG cylinder had a diameter of 25 mm and a thickness of 5 mm. PETG was chosen because its relative permittivity is similar to that of mineral oil. The second GRIN lens used for beam-steering was made thinner (by 2 mm) so that the delay through the cylinder and the thinner lens at boresight was like that of the GRIN lens. Here beam-steering was seen by moving the cylinder away from the center of the lens. This movement of the dielectric cylinder represents the action of an oil droplet that could be allowed to move on the inner surface of the lens to counteract any axial vibrations of the antenna, as the oil droplet would move in the opposite direction of the antenna by inertia. This steers the beam opposite the direction of perturbation to cancel it. To realize this with oil, additional layers of dielectric material would be needed to contain the droplet and aid in keeping the droplet's neutral state in the center of the lens. This work uses a solid dielectric cylinder to emulate this effect.

Fabrication – The horn is fed with an off the shelf coaxial to WR-42 waveguide launcher (Pasternak PE9878) and was 3D printed using PLA on a Dremel 3D45 3D printer. The horn was printed in four sections so that the joints between each section were in the corners of the waveguide and the copper tape could easily be applied to the inner surface of the horn. The wider $\vec{E}$-field (Fig. 2(a)) walls of the waveguide had a threaded flange to attach the launcher. Both walls had a groove to receive the thinner $\vec{H}$-field walls (Fig. 2(b))

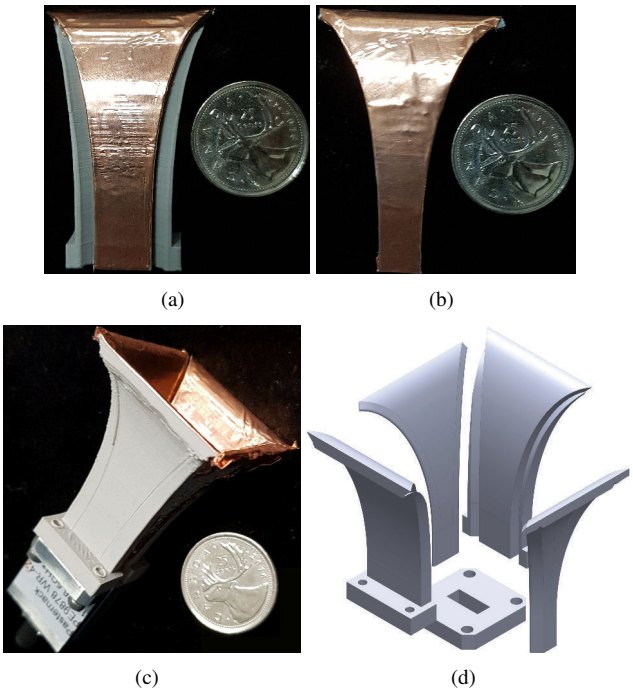

Figure 2. Segments of the 3D printed WR-42 horn antenna covered in copper tape. (a) $\vec{E}$ wall of the horn, (b) $\vec{H}$ wall of the horn, (c) the assembled horn connected to the WR-42 waveguide launcher. (d) CAD exploded view showing the how the horn walls connect

between them. The assembled horn was held together by the launcher as seen in Fig. 2(c), Fig. 2(d) shows the joints in detail.

The permittivity of the GRIN lens was varied by changing the volumetric fill of each unit cell as seen in Fig. 3(a). The lens was printed with 2 mm by 2 mm unit cells to match the shell thickness in the simulated lens. To get a lower permittivity than could be printed with the 2 mm by 2 mm unit cell, a larger unit cell of 4 mm by 4 mm was used at the edges of the lens.

The PETG cylinder in Fig. 3 (b,c) was adhered to the pocketed lens using a piece of thin, double-sided PDMS (polydimethylsiloxane) adhesive, ARseal 90880. The full setup is seen in Fig. 3(d) where the lens is supported at the desired offset distance using a mount that is printed out of PETG with posts at the corners of the waveguide to not shadow the lens or horn in the principal radiation cut planes.

3 Measured Results

Measured input reflection data was taken using an Anritsu MS4644B vector network analyzer and radiation pattern data was collected using the anechoic chamber at Queen's University. Fig. 4 shows the measured and simulated input reflection for the horn measured through the WR-42 launcher for the horn and the horn with the lens from 18 GHz to 28 GHz. The horn without the lens saw an input

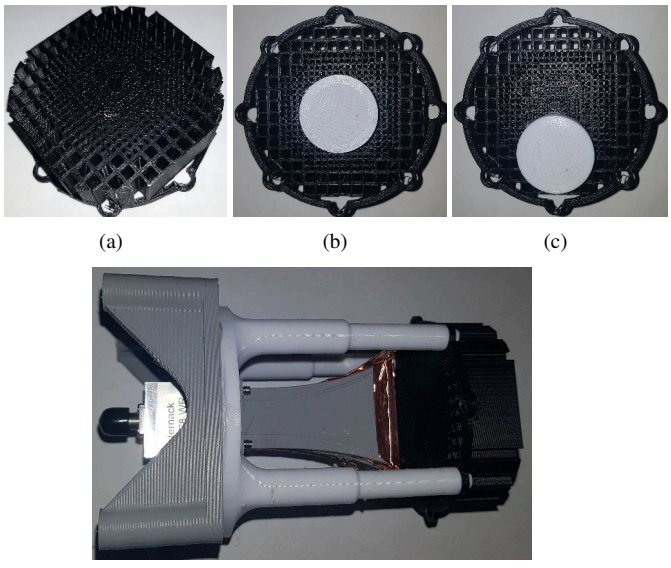

(a) (b) (c)

(d)

Figure 3. (a) 3D printed GRIN lens, (b) Pocketed GRIN lens with a PETG cylinder located on the horn side of the lens at the center of the lens, (c) PETG cylinder offset to the side of the lens by 12.5 mm, (d) Horn and full thickness lens on the horn antenna with WR-42 launcher and lens support

reflection better than -13 dB across the band. The addition of the lens increased the reflected power, while remaining below -10 dB.

Fig. 5 shows the measured and simulated peak realized gain and peak directivity across the band for the horn with no lens. Here the measured and simulated peak directivity for the horn are similar across the band, but the measured peak realized gain is lower than what was simulated. This decrease in gain is likely attributed to the surface roughness of the copper tape on the 3D printed horn that can be seen in Fig. 2.

Fig. 6 shows the measured peak realized gain for the horn, horn and lens, and the steering setups with the pocketed lens. Here the lens contributes a minimum of 5 dB gain increase over the horn across the band. The pocketed lens, and the steering cases where the cylinder was moved showed very similar levels of peak gain.

Radiation patterns at two frequencies are shown in in Fig. 7 for the horn, horn and lens, and the horn with the pocket lens with the PETG cylinder in the center of the lens. The beam-forming characteristics of the lens can be seen, as well as the impact of the pocketed lens with the cylinder at the center. The delay through the outer edge of the thinner lens is less that that of the full GRIN lens. Regardless, the beam-forming characteristics are similar for the main lobe, with a slightly larger side-lobe response around the first null.

Next the measured beam-steering is shown across the band for the pocketed lens when the PETG cylinder is moved.

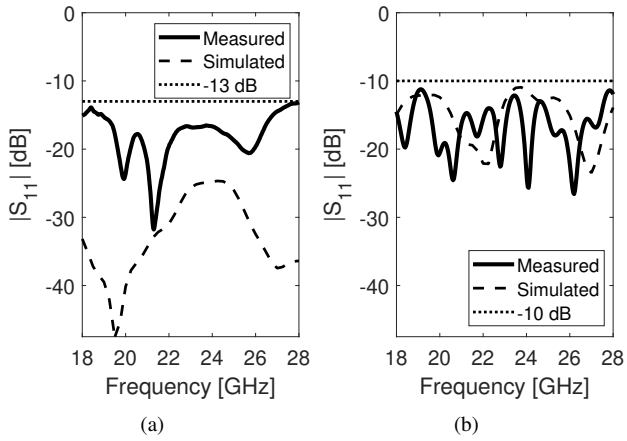

(a) (b)

Figure 4. Measured and simulated input reflection for the (a) horn, and (b) horn and lens

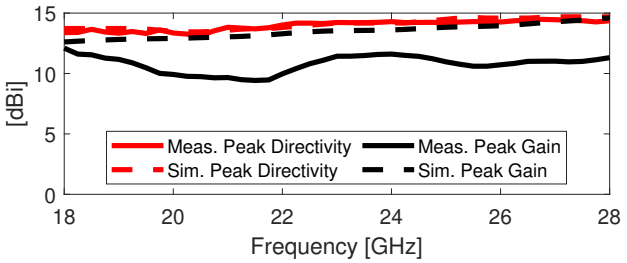

Figure 5. Measured and simulated peak realized gain and directivity for the horn showing the impact of the surface roughness in the copper tape

For each setup shown in Fig. 8 the cylinder was moved from the center of the lens in the listed direction by the radius of the cylinder (12.5 mm). The beam-steering is consistent across the band in all directions at $\pm$ 5°. The radiation patterns demonstrating this steering are included in Fig. 9. For simplicity, co-polarization radiation patterns are only shown in the direction of steering. The peak gain for each of the steered beams is comparable to the centered cylinder.

4 Conclusion

This work showed the design of a 3D printed horn with a GRIN lens that covered 18 GHz to 28 GHz. This GRIN lens gave a gain increase of more than 5 dB across the band. The beam-steering GRIN lens and PETG cylinder showed a method for counteracting axial perturbations for narrow beamwidth antennas by providing $\pm$ 5° of beam-steering.

Acknowledgements

This work was supported, in part, by grant #STPGP-521223-2018 from the Natural Sciences and Engineering Research Council of Canada (NSERC). I. Goode is a recipient of the Ontario Graduate Scholarship from the Province of Ontario, Canada, and the Ian M. Drum Scholarship from Queen's University.

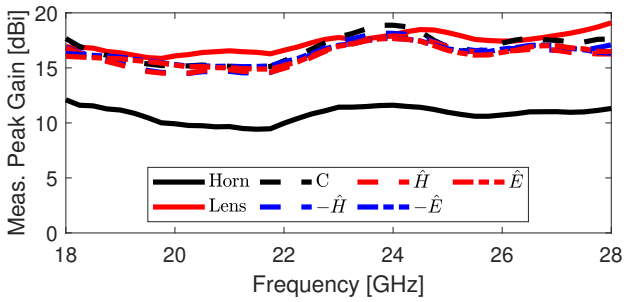

Figure 6. Measured peak realized gain for the horn, horn and lens, and the positive and negative directions from boresight in the $\hat{E}$ and $\hat{H}$ field cut directions and the centered cylinder "C" all with the PETG cylinder on the pocketed lens

References

[1] K. V. Hoel, M. Ignatenko, S. Kristoffersen, E. Lier, and D. S. Filipovic, "3-d printed monolithic grin dielectric-loaded double-ridged horn antennas," *IEEE Trans. Antennas Propag.*, vol. 68, no. 1, pp. 533–539, 2019.

[2] K. Lomakin, T. Pavlenko, M. Ankenbrand, M. Sippel, J. Ringel, M. Scheetz, T. Klemm, D. Gräf, K. Helmreich, J. Franke, *et al.*, "Evaluation and characterization of 3-d printed pyramid horn antennas utilizing different deposition techniques for conductive material," *IEEE Trans. Compon. Packag. Manuf. Technol*, vol. 8, no. 11, pp. 1998–2006, 2018.

[3] Y. Li, L. Ge, M. Chen, Z. Zhang, Z. Li, and J. Wang, "Multibeam 3-d-printed luneburg lens fed by magnetoelectric dipole antennas for millimeter-wave mimo applications," *IEEE Trans. Antennas Propag.*, vol. 67, no. 5, pp. 2923–2933, 2019.

[4] B. Zhang, Y.-X. Guo, H. Zirath, and Y. P. Zhang, "Investigation on 3-d-printing technologies for millimeter-wave and terahertz applications," *Proc. IEEE*, vol. 105, no. 4, pp. 723–736, 2017.

[5] H. Banting and C. E. Saavedra, "Dielectric spectroscopy of fluids and polymers for microwave microfluidic circuits and antennas," *IEEE Trans. Microw. Theory Techn.*, vol. 69, no. 1, pp. 337–443, 2021.

[6] K. Lomakin, T. Pavlenko, M. Sippel, G. Gold, K. Helmreich, M. Ankenbrand, N. Urban, and J. Franke, "Impact of surface roughness on 3d printed sls horn antennas," in *European Conf. Antennas Propag.*, pp. 1–4, 2018.

[7] Z. Khan, H. He, X. Chen, and J. Virkki, "Dipole antennas 3d-printed from conductive thermoplastic filament," in *IEEE Electron. Syst. Integr. Technol. Conf.*, pp. 1–4, IEEE, 2020.

[8] D. Helena, A. Ramos, T. Varum, and J. N. Matos, "Inexpensive 3d-printed radiating horns for customary things in iot scenarios," in *European Conf. Antennas Propag.*, pp. 1–4, IEEE, 2020.

[9] I. Goode and C. E. Saavedra, "Millimeter-wave beam-steering antenna using a fluidically reconfigurable lens," *IEEE Trans. Antennas Propag.*, pp. 1–6, 2020.

[10] B. Fuchs, L. Le Coq, O. Lafond, S. Rondineau, and M. Himdi, "Design optimization of multishell luneburg lenses," *IEEE Trans. Antennas Propag.*, vol. 55, no. 2, pp. 283–289, 2007.

[11] B. Zhou, Y. Yang, H. Li, and T. J. Cui, "Beam-steering vivaldi antenna based on partial luneburg lens constructed with composite materials," *J. Appl. Phys*, vol. 110, no. 8, p. 084908, 2011.

[12] Y. He and G. V. Eleftheriades, "Matched, low-loss, and wideband graded-index flat lenses for millimeter-wave applications," *IEEE Trans. Antennas Propag.*, vol. 66, no. 3, pp. 1114–1123, 2018.

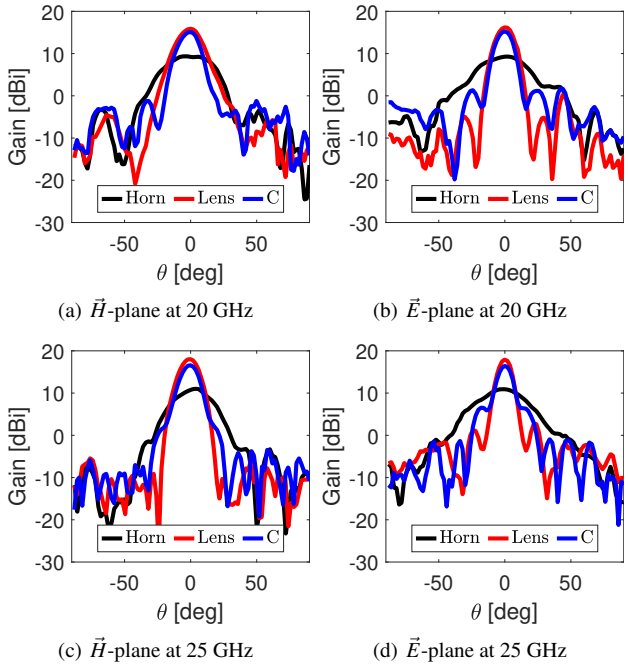

(a) $\vec{H}$-plane at 20 GHz (b) $\vec{E}$-plane at 20 GHz

(c) $\vec{H}$-plane at 25 GHz (d) $\vec{E}$-plane at 25 GHz

Figure 7. Measured realized gain radiation patterns at various frequencies in the two principal radiation cuts for the horn, horn and lens, and horn and pocketed lens with the PETG cylinder at the center of the lens ("C")

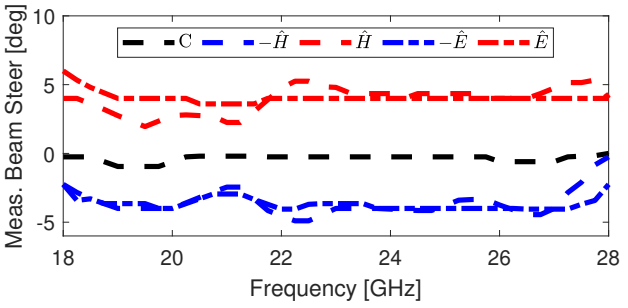

Figure 8. Measured beam steering for the perturbation of the PETG cylinder

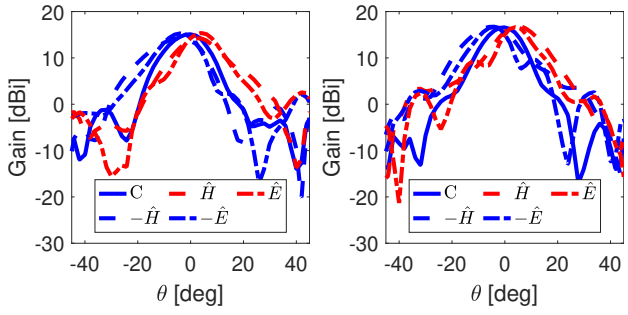

(a) 20 GHz (b) 25 GHz

Figure 9. Measured realized gain radiation patterns at various frequencies showing the beam-steering for the perturbation of the PETG cylinder. Each pattern is in the plane corresponding to the direction of beam-steering